Autonomous stochastic resonance in bursting neurons

André Longtin
Département de Physique, Université d'Ottawa, 150 Louis Pasteur, Ottawa, Ontario, Canada K1N 6N5
(Received 29 July 1996)

Noise-induced firing is studied in two major classes of bursting neuron models in the absence of periodic input. In the biologically relevant subthreshold regime where no deterministic firing occurs, additive noise induces spiking limit cycles. This noise makes the output firing patterns sensitive to the characteristics of autonomous subthreshold oscillations, which can change in response to various physicochemical stimuli. The nonmonotonic behavior with increasing noise of the phase locking between spikes and subthreshold oscillations, measured using spectral signal-to-noise ratios and line shape characteristics, are a manifestation of autonomous stochastic resonance in these systems. The type of bifurcation giving rise to bursting activity determines the behavior with noise of the mean firing frequency, interspike interval histogram, spike train power spectrum, and phase locking. In particular, it is shown that a saddle-node bifurcation is not required to see stochastic resonance (SR) without periodic input when there exists a stable deterministic subthreshold oscillation. This paper also studies SR in a detailed ionic neuron model, an approach that leads to tests of hypotheses regarding the nature of noise in real neurons. [S1063-651X(97)12001-3]

PACS number(s): 87.22.Jb, 05.40.+j

I. INTRODUCTION

There has been much recent work on stochastic resonance (SR) in excitable neural systems [1]. Work on SR in neurobiology has shown that noise helps neurons fire near a preferred phase of small amplitude external periodic stimuli, giving them the ability to detect subthreshold signals. At the same time, major advances in neural dynamics and computation have highlighted the potential importance of neuronal oscillations as carrier signals for coding mechanisms [2]. These mechanisms rely on the timing of firing events (''spikes'') with respect to single neuron or network oscillations. These studies have emphasized that autonomous subthreshold and bursting oscillations (Fig. 1) are key elements of neural coding. The generation of network oscillations with noise as an essential factor [3], and the influence of noise on the timing of spikes with respect to external signals [4] have previously been investigated. However, the possibility that noise may enhance timing with respect to autonomous rhythms has received little attention.

Recent experimental [5] and modeling [6] studies of temperature receptors in certain mammals and electric field receptors in certain fish have concluded that firing patterns from such neurons are generated by the interplay of subthreshold oscillations and noise. These studies have suggested that such neurons may exhibit SR *without external forcing*. SR without external forcing has recently been studied in a simple dynamical system right at a saddle-node bifurcation [7]. The noise-induced limit cycle and the noise-induced shifts of its mean frequency are consequences of the nonuniformity of the cycle, and of the dependence on noise of the first passage time for such bifurcations [8,9].

The present paper shows that bursting neuron models, biased into the subthreshold regime as in [5,6], indeed exhibit novel types of *autonomous* SR. The noise-enhanced phase locking of spikes is discussed here for two important classes of bursting dynamics [10]. In the first class, which we refer to as the ''slow wave'' case, the full dynamics separate into a fast subsystem, which produces spikes, and a slow subsystem, which oscillates autonomously and independently of the occurrence of spikes. ''Bursts'' or groups of spikes arise when the slow wave oscillation brings the membrane voltage past the activation threshold for the fast currents underlying the generation of spikes (see Fig. 1). This slow oscillation would persist even if one or more of these fast currents were inhibited. The Plant model [11] is chosen here as a representative of this class. Below, we study this model with additive

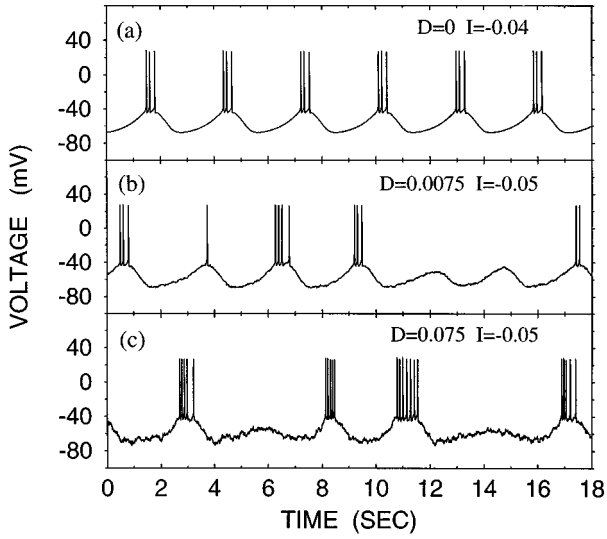

FIG. 1. Membrane voltage vs time for Plant's model of ''slow wave'' bursting [Eqs. (1)–(6)]. (a) Periodic suprathreshold solution for $D=0$ and $I=-0.04$. (b) A subthreshold solution with $D=0.0075$ and $I=-0.05$: noise is required to produce spikes. (c) Same as (b), but $D=0.075$. The numerical integration time step is 6.25×10^{-2} msec. Parameters are $\lambda=4.0$, $\rho=0.0017$, $G_I=7.84$, $G_x=0.01$, $G_K=0.363$, $G_C=0.03$, $G_L=0.003$, $K_c=0.0085$, $V_I=30$, $V_K=-75$, $V_L=-40$, $V_C=140$, $C_M=1$, $\tau_x=235$, and $t_c=1.0$ msec. Other parameters and voltage dependencies are as in [11]. All these parameters produce solutions where voltage is in millivolts and time is in milliseconds.

noise in the regime where the slow wave has a large amplitude, but is slightly subthreshold for the fast dynamics; in other words, no spikes are generated in the absence of noise. This is the biologically relevant case [5,6]. We find that this stochastic model exhibits genuine autonomous SR without the requirement of a nonuniform limit cycle, in contrast with previous studies [7,8].

In the second class, bursts are driven by spikes, and thus we have the label ''spike-driven'' bursting. This label means that the alternation between an active phase, during which many spikes are generated in fast succession, and a quiescent phase where no spikes occur, requires the occurrence of spikes. The spikes produced during the active phase cause variations in one or more slow variables, with the result that the mean membrane potential is progressively lowered until spikes can no longer be generated. The membrane potential then increases slowly during this quiescent phase, until rapid firing resumes, and the cycle repeats. The specific model used, the Hindmarsh-Rose (HR) model [12], has recently been studied in the chaotic bursting regime in the context of synchronized oscillations in networks of cortical neurons [13]. Some of the features of the noise-induced firing in this model are shown here to be similar to those reported in [7].

Our results are also a demonstration of SR in a detailed Hodgkin-Huxley-type ionic model of neuron firing, an important step in characterizing the influence of various noise sources on the dynamics of real neurons. Our findings clearly indicate that neurons in the two classes described above can sharpen their timing as the intensity of noise increases over a certain range. This noise can be due to intrinsic conductance fluctuations in the membrane of the neuron [6], as well as to stochastic (see, e.g., [14]) and/or chaotic [13] synaptic currents.

The paper is organized as follows. Section II presents the stochastic Plant model, a Hodgkin-Huxley-type ionic model of autonomous slow wave bursting biased into a subthreshold regime. Numerical integration results for time series distributions of interspike intervals and spike train power spectra are also discussed in Sec. II. Section III presents the Hindmarsh-Rose model of bursting near a saddle node, and the associated interval distributions and spike train power spectra. It also discusses the difference in phase locking for the two models of interest. Results on autonomous stochastic resonance in both models are then presented in Sec. IV. Section V offers a characterization of the firing statistics, and discusses the relevance of recently proposed theories to this characterization. The paper concludes with Sec. VI.

II. NOISE-INDUCED BURSTING FROM A SLOW WAVE

A. Model

The Plant model of slow wave bursting [11] with additive stochastic forcing, used to model thermoreceptors [6], is governed by the following equations:

$$C_M\dot{V}=G_I m_\infty^3(V)h(V_I-V)+G_x\,x(V_I-V)+G_K n^4(V_K-V)+G_C\,\frac{C}{0.5+C}\,(V_K-V)+G_L(V_L-V)+I+\eta(t), \quad (1)$$

$$\dot{h}=\lambda[h_\infty(V)-h]/\tau_h(V), \quad (2)$$

$$\dot{n}=\lambda[n_\infty(V)-n]/\tau_n(V), \quad (3)$$

$$\dot{x}=\lambda[x_\infty(V)-x]/\tau_x, \quad (4)$$

$$\dot{C}=\rho[K_c x(V_C-V)-C], \quad (5)$$

$$\dot{\eta}=-\frac{1}{t_c}\,\eta+\frac{1}{t_c}\,\xi(t). \quad (6)$$

$V(t)$ is a fast variable representing the membrane voltage, h,n,x are gating variables, C is the intracellular calcium concentration, and I is a bias current. $\eta(t)$ is a zero-mean Ornstein-Uhlenbeck (OU) process with correlation time t_c and autocorrelation function $\langle\eta(t)\eta(s)\rangle=(D/t_c)\exp(-|t-s|/t_c)$. The other parameters and the detailed voltage dependencies of τ_h, τ_n, h_∞, n_∞, m_∞, and x_∞ are as in Ref. [11]. In the following, we refer to the noise intensity as D.

B. Numerical integration method

We now discuss the numerical integration of our model equations. There are different methods to integrate the stiff deterministic system Eqs. (1)–(5). Best results are usually obtained with implicit schemes, which allow the use of a reasonable time step, all the while ensuring solution stability (see, e.g., [15]). However, one must proceed very cautiously for the integration of these equations in the presence of noise, in order to ensure proper sampling of the stochastic forces. In general this can be achieved using an explicit fixed-step method [16]. Our conservative approach to this stiff stochastic system is thus based on the method discussed in [16] for systems driven by colored noise. It involves integrating Eqs. (1)–(6) using a fixed-step explicit scheme for Eqs. (1)–(5), coupled to an integral Euler algorithm for the integration of the stochastic OU process. This numerical integration of the Gaussian white noise in Eq. (6) produces the colored OU noise, which, due to its simple additive coupling to the voltage dynamics Eq. (1), acts as a driving force on the deterministic system Eqs. (1)–(5). The algorithm in [16] is well adapted to this kind of coupled dynamics.

However, since the deterministic system is stiff, it is important to use such an explicit method with a very small time step in order to obtain accurate spike times. This time step must be small enough to properly integrate the noise process (in general, it must be smaller than the noise correlation time), and produce a solution to the deterministic system with the required accuracy for the study of the phenomena of interest. The time step must also produce sufficient accuracy for properties of the stochastic system, such as the interspike interval histogram, or mean interspike interval (see below). All these factors lead to lengthy simulations. We have found that the simple Euler forward scheme produces the required accuracy for a time step of $t_c/16=0.0625$ msec. It was found to be more accurate for the stochastic case than the fourth-order Runge-Kutta method for an equivalent computation time, even though both methods produce practically identical deterministic solutions for both the bursting and nonbursting cases.

The phenomenon described in our study, i.e., the behavior of the stochastic phase locking as a function of noise inten-

sity, can already be seen for time steps as large as 0.5–1 msec. For these and smaller time steps, the deterministic solutions and the properties of the stochastic solutions show clear convergence; i.e., the percentage in variation of solutions and properties decreases as the time steps are halved. The time step we have chosen, 0.0625 msec, provides greater accuracy than those of 0.5–1 msec; it produces 320 integration steps for the approximately 20-msec action potential.

The accuracy of the solutions using this 0.0625-msec time step was assessed by integrating the deterministic equations (with zero noise) with a slightly different value of I ($I=-0.04$ instead of -0.05), producing deterministic bursting with three spikes per burst [Fig. 1(a)]. The corresponding interspike intervals (ISI's) were 2604.4, 112.7, and 147.9 msec. Halving the time step to 0.03125 yielded new ISI's, which differed from these by, respectively, 0.3%, 1.1%, and 3%. The ISI that dominates the behaviors studied below, such as the power at the basic frequency of the noise-induced bursting, is the long one corresponding to the duration of the quiescent phase. Since the variation of this ISI is very small, and since the other ISI variations are also small, we have used the time step of 0.0625. Our integration method shows clear convergence of ISI's to almost identical values upon halving the step further and further.

In the presence of noise, the effect of halving the step size on the spike times can of course only be assessed in a statistical sense. This follows from the fact that halving the time step requires twice as many ''noise'' values, and the realization is thus different from the original one with the larger time step. We have found that the ISI histograms (ISIH's) obtained using different small time steps have qualitatively similar shapes. This is basically true for the power spectra also, namely, for the power in the fundamental peak (see below), but smaller time steps reveal more detailed structure in the spectra. The effect of the time step on the mean ISI (see below) was found to produce larger variations than in the deterministic case. For example, for a midrange noise intensity $D=0.01$, halving the time step produces a mean ISI within 1.5% of the one for the 0.0625 time step (2545 msec), but further reduction produces a convergence toward a value within 15% of 2545. This is true for the mean ISI with and without bursts (see below). This and other tests suggest that 15% is a conservative estimate of the error on signal-to-noise ratios and mean ISI's calculated below. Of interest also is the fact that the mean ISI values obtained for a given time step but for different sets of realizations fluctuate statistically with a standard deviation of approximately 1%.

Clearly, higher accuracy can be achieved with time steps smaller than 0.0625 msec and, most likely, higher accuracy and computational efficiency could be achieved using suitably tested more sophisticated algorithms. This is beyond the scope of our study. Our aim, achieved with the integration scheme we have chosen, is to illustrate the basic phenomenology of noise-induced firing in two classes of bursting cells with a given high level of accuracy. Our results do not change qualitatively with smaller time steps.

A deterministic solution of Eqs. (1)–(6) (i.e., a solution with $D=0$) is shown in Fig. 1(a). One can see fast spikes occurring on top of a slow wave. This system is decomposable into a fast subsystem (V,h,n), and a slow subsystem (x,C) that oscillates autonomously [17]. For zero noise intensity $D=0$, spikes occur provided this ''slow wave'' reaches the activation threshold of the fast spiking dynamics. The fixed point (no firing) to limit cycle (repetitive firing) transition in the fast dynamics is of the homoclinic type [17]. A bursting pattern occurs because the slow wave moves the fast dynamics from fixed point to limit cycle and back.

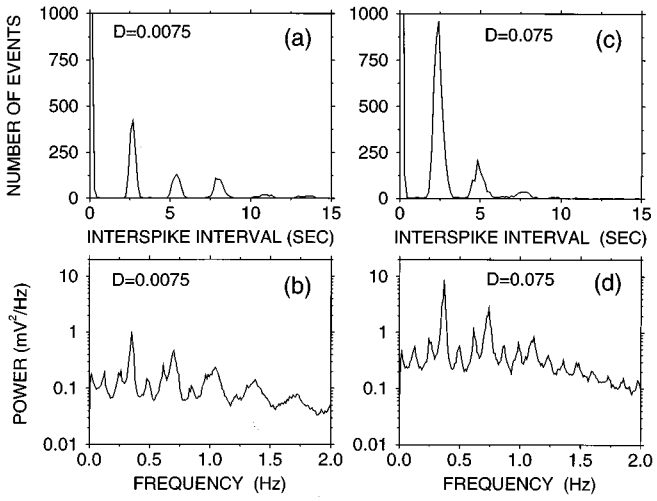

FIG. 2. Interspike interval histograms and spike train power spectral densities from simulations of Eqs. (1)–(6) with $I=-0.05$. (a), (b) $D=0.0075$. (c), (d) $D=0.075$. For each noise intensity, 100 realizations were used to generate 200-bin histograms and (0, 10) Hz spectrum averages. Parameters and time step are as in Fig. 1. A spike is counted if it reaches 0 mV. In each realization, statistics were computed, after 8×10^5 time steps of transients, over a 204.8-sec window formed by the next 3.3×10^6 time steps. 4096-point Hanning-windowed fast Fourier transforms were computed using spike trains resampled at 0.05 sec [21] (Nyquist frequency $f_s=10$ Hz), a value smaller than the smallest computed interval.

C. Interspike interval histograms and power spectra

We now discuss the parameter range of interest. The physiologically relevant cases are the suprathreshold case where bursting occurs, and also the subthreshold case where ''skipping'' occurs. Skipping is a form of stochastic phase locking in which neuron firings occur near a given phase of some periodic forcing, but are separated by a random integer number of cycles of this periodic forcing. In the context of the five-dimensional Plant model, the slow wave of the slow subsystem in some sense acts as a periodic forcing on the fast dynamics. In Fig. 1(b), the bias current is $I=-0.05$, and the slow wave is subthreshold: spikes occur only for $D>0$. They appear in bursts of one or more near the crest of the slow wave, their number increasing with D.

Figures 2(a) and 2(c) show ISIH's computed from many different realizations of the stochastic Plant model. Intervals at integer multiples of the slow wave period are seen, as well as short intervals measured between successive spikes inside a ''burst.'' It is clear from these results that firings are phase locked to the slow wave, and groups of spikes or ''bursts'' are separated by a random number of slow wave cycles. The mean number of slow wave periods skipped between bursts decreases as D increases [Figs. 2(a) and 2(c)], a familiar feature of systems that display SR [18,19].

The phase locking of spikes to the subthreshold slow wave can also be analyzed using spike train power spectra. Based on previous studies [20], the spectra of noise-induced bursting solutions are expected to have an intricate structure of harmonics and sidebands. Each spike in a realization was convolved with $\sin(2\pi f_s t)/(2\pi f_s t)$, and then resampled using f_s as the Nyquist frequency. This method [21] produces spectral estimates that are alias-free across a spectrally flat window $(0,f_s)$. The low frequency portion of power spectra, computed from the same realizations as the corresponding ISIH's, are shown in Figs. 2(b) and 2(d). Harmonics of the mean slow wave frequency $f_0=1/T_0$ are seen over a curved background, along with pairs of peaks between these harmonics, which are most likely noisy precursors of a Hopf bifurcation [22].

The signal peaks are broad when compared to simulations of externally forced stochastically resonant systems (see, e.g., [1,23,25]). This is due to the fact that the dynamics are autonomous and driven by noise. This leads to phase fluctuations in the slow wave, a phenomenon known to broaden peaks at harmonics of the signal frequency [26]. We note that there are two kinds of phase averagings in our computations: an ''intrinsic'' one, due to the noise itself, and another one, added to our simulation code, which produces phase-averaged power spectra. This latter averaging is done for each realization by shifting the spike train by a random fraction of the mean slow wave period T_0. This averaging is useful in comparing simulations with experimental results in which the phase of the slow wave is different at the beginning of each spike train measurement. It would be practically impossible, especially at higher noise levels, to experimentally control for this phase, in contrast with the case of external forcing.

At higher noise levels, this second averaging is not necessary in principle, especially if long transients are discarded, since the phase of the slow wave becomes randomized by the noise during the temporal evolution (again in contrast to externally forced systems). At low noise, the phase of the slow wave is not significantly perturbed by the noise, and thus the ''added'' averaging helps. The spectral peaks are nevertheless broad at low noise because only a small number of spikes occur in a given realization. These considerations also apply to the HR model investigated in the next section.

III. NOISE-INDUCED BURSTING NEAR A SADDLE-NODE BIFURCATION

A. Model

We now investigate noise-induced firing from the subthreshold regime in another important class of bursting neuron dynamics. The Hindmarsh-Rose model [12] typifies ''spike-driven'' bursting [10]:

$$\dot{x}=y-ax^3+bx^2+i-z+\eta(t), \tag{7}$$

$$\dot{y}=c-dx^2-y, \tag{8}$$

$$\dot{z}=r[s(x-x^*)-z]. \tag{9}$$

Note that the HR model in [12] was extended here by adding an OU process η to the dynamics of the fast voltage variable x, as was done for the Plant model in Sec. II. This model, in contrast with the one studied in the previous section, does not have a deterministic slow subsystem that can oscillate in the absence of spikes. Without noise and in the suprathreshold regime, spikes always accompany the slow oscillation, a consequence of the particular bifurcation structure of the deterministic flow. In contrast, the spikes can be eliminated in the suprathreshold regime of the Plant model, e.g., by setting $G_I=0$ in Eq. (1).

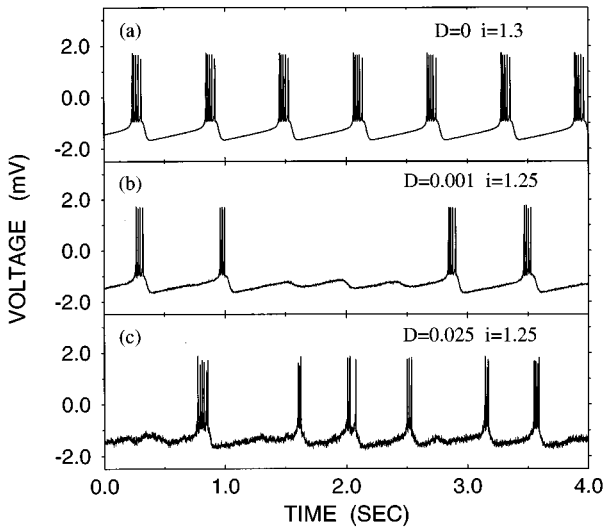

FIG. 3. Membrane voltage vs time for the Hindmarsh-Rose model of ''spike-driven'' bursting [Eqs. (7)–(9)]. (a) Periodic suprathreshold solution for $D=0$ and $i=1.3$. (b) A subthreshold solution with $D=0.001$ and $i=1.25$: noise is required to produce spikes. (c) Same as (b), but $D=0.025$. The numerical integration time step is 6.25×10^{-3} msec. Parameters are $a=1$, $b=3$, $c=1$, $d=5$, $s=4$, $r=0.001$, $x^*=-1.6$, $i=1.25$, and $t_c=0.1$ msec. These parameters produce solutions where voltage is in millivolts (scaled with respect to experimental values) and time is in milliseconds.

B. Numerical integration method

The discussion in Sec. II B on the choice of numerical methods also applies to the equations in this section. The fixed step Euler forward scheme coupled to the integral Euler scheme for the OU process [16] was used as in Sec. II B for the same reasons. The accuracy of the spike times in the absence of noise was checked as in the previous section, i.e., by slightly changing the bias current i from the subthreshold case value 1.25 to the suprathreshold case 1.30. With the chosen time step of 0.00625, this yields a solution with five spikes per burst, with ISI's of 535.5, 15.1, 17.1, 20.8, and 36.0 msec [Fig. 3(a)]. As in Sec. II B, we have found a clear convergence of all solutions, and thus of the ISI's, as time steps are successively halved. This convergence is seen starting from time steps eight times as large as 0.00625. With a time step of 0.003125, the long ISI corresponding to the duration of the quiescent phase, which is the most important ISI from the point of view of our characterization of noise-induced firing, varied by 0.28%, while the others varied by 3.2%, 4.1%, 6.3%, and 21%, respectively. Comparison to a simulation with a time step 128 times smaller than 0.00625 yielded variations of, respectively, 0.15%, 6.2%, 7.8%, 11%, and 32%. The higher error in the last ISI is expected from the

slowness of convergence of the solution due to the crossing of a saddle-node bifurcation into the quiescent phase.

In the presence of noise, we have found that the variations in mean ISI upon halving the time step from 0.00625 to 0.003125 are smaller than for the previous model in Sec. II B. For example, for $D=0.01$, the mean ISI goes from 176 to 161 msec, a 9% variation. Our tests indicate that the error on mean ISI's and signal-to-noise ratios calculated below are probably lower than 15%, our estimate for the Plant model. We note that the mean ISI's without bursts (see below) vary less (2–3%) than in the stochastic Plant model upon halving the time step. The statistical error on these mean ISI's is again on the order of 1%, as for the Plant model.

The neurophysiologically relevant regime for this system is again the case where bursting occurs, and also the subthreshold case where deterministic firing is not possible. If the bias parameter $i>1.26$, the deterministic dynamics are suprathreshold, and the slow variable z causes periodic crossings of a saddle-node bifurcation. This produces a slow alternation between two globally stable attractors: a fixed point and a fast limit cycle. A relaxation-type bursting oscillation then ensues, as shown in Fig. 3(a) for $i=1.3$. The subthreshold case of interest in our study is characterized by the absence of a deterministic limit cycle. This subthreshold regime is achieved when $i<1.26$; noiseless solutions then converge in an oscillatory manner to a globally stable fixed point (i.e., the linearization around the fixed point has a pair of complex conjugate eigenvalues). Noise can then induce bursting sequences, and the mean time between groups of spikes decreases as the noise intensity increases, as seen by comparing Fig. 3(b) and Fig. 3(c).

C. Interspike interval histograms and power spectra

Interspike interval histograms and spike train power spectra were also computed in the same manner as those for the Plant model. They are shown at two noise amplitudes in Fig. 4. In comparison to the slow wave case in Figs. 2(a) and 2(c), the ISIH modes at integer multiples of the slow time scale of bursting for the noisy HR model are less clearly defined; in particular, one does not see many modes separated by interval ranges where no events occur. In other words, the phase locking of the noisy excitable dynamics of HR to its internal slow time scale is weaker than in the autonomous slow wave case of the Plant model.

The reason for this difference in the degree of phase locking is that the slow time scale in the subthreshold HR case, which is strongly dependent on r (increasing r shortens the bursting period in the suprathreshold regime), is not as sharply defined as in the Plant model. In the Plant model, the slow wave is self-sustained on a two-dimensional submanifold, with or without noise. This slow wave is much more stable to noise, except if it is about to disappear at some bifurcation in the slow dynamics [17,6], which is not the case here. Further, its high stability is not affected by the fact that the transition from fixed point to limit cycle in the fast subsystem is of the homoclinic type. Hence the slow time scale is sharp even in the presence of noise, which leads to strong phase locking when the system is subthreshold. However, for the subthreshold HR case, the slow time scale is not so sharply defined since we are in the presence of a noise-induced limit cycle that does not have a deterministic counterpart. Its sharpness depends on the noise (see Sec. IV), but also on the fixed point dynamics and of course on the fact that the dynamics undergo a global saddle-node bifurcation at the threshold for bursting (the period is infinite at such a bifurcation) [7–9].

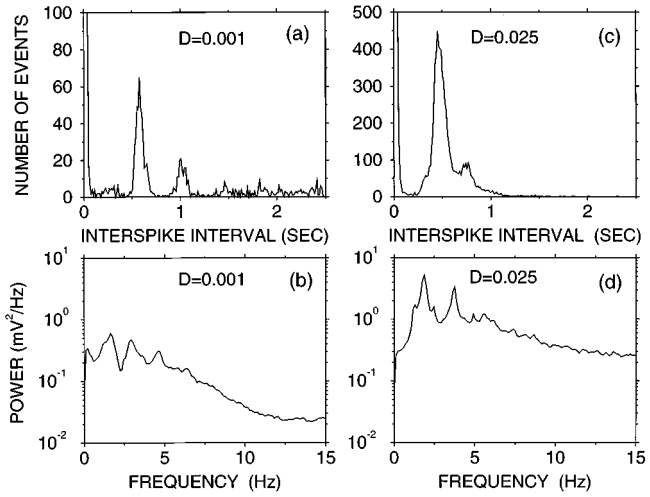

FIG. 4. Interspike interval histograms and spike train power spectral densities for the Hindmarsh-Rose model [Eqs. (7)–(9)] with $i=1.25$. (a), (b) $D=0.001$. (c), (d) $D=0.025$. For each noise intensity, 100 realizations were used to generate 200-bin histograms and (0, 120) Hz spectrum averages. In each realization, statistics were computed using 2.7×10^6 time steps (17.1-sec window) following 2×10^5 time steps of transients. Parameters and time step are as in Fig. 3. A spike is counted if it reaches 1 mV. The spectra were computed as in Fig. 2, but with a Nyquist frequency of 120 Hz.

IV. AUTONOMOUS STOCHASTIC RESONANCE

The dependence on D of the fundamental mean frequency f_0 and of the phase locking for both models is contrasted in Figs. 5 and 6. Figure 5 shows spike train power spectra at low frequency, calculated from the Plant model for increasing noise intensity. The highest peak in each spectrum corresponds to f_0. This frequency is seen to be almost constant over three orders of magnitude of D, since the slow wave, which arises from a Hopf bifurcation in the slow subsystem, exists even without noise in the subthreshold regime [17,6].

Spectra from the HR model for increasing D are shown in Fig. 6. The main peak at f_0 is clearly broader than the one for the Plant model, a consequence again of the noise-induced nature of the limit cycle. Further, f_0 increases with D over the range of noise intensities studied, as seen in [7], although the increase is minimal at the higher D values used. We anticipate that f_0 will decrease at even higher noise levels, following the behavior seen in [7], but it is likely that the meaning of the results will then be questionable since action potentials will be strongly distorted. At high D, a sharpening of the $2f_0$ harmonic is seen, due to interspike intervals near multiples of $T_0/2$. These arise because the complex eigenvalues at the fixed point cause oscillations between bursts with a period near these multiples.

Figure 5 also shows that the fundamental peak sharpens at $D\approx0.075$ for the Plant model, while Fig. 6 shows the same

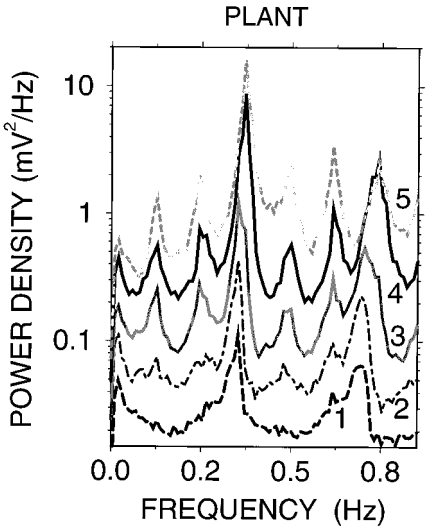

FIG. 5. Spike train power spectral densities computed from 100 realizations of the Plant model at each of the following values of noise intensity D: 0.00075 (1), 0.0025 (2), 0.01 (3), 0.075 (4), and 0.5 (5). Other parameters are as in Fig. 1. Only the lower frequency part of the spectra is shown on these lin-log plots.

for the HR model at $D \approx 0.025$. These ''resonances'' can be analyzed using the signal-to-noise ratio (SNR) [1] and the degree of coherence β [7]. This latter quantity is defined as the peak height h divided by its relative width, $\Delta f/f_0$, where Δf is the peak width at half maximum. Results are shown in Fig. 7(a) for the Plant model and in Fig. 8(a) for the HR model. It is important to point out that, for both models, the breadth of the f_0 peaks and the presence of secondary peaks complicates the estimation of signal-to-noise ratios (see Fig. 7), and is responsible for significant uncertainties (± 1 dB) at the highest noise levels shown.

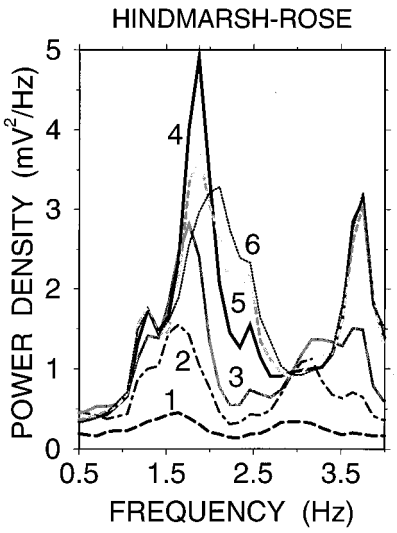

FIG. 6. Spike train power spectral densities computed from 100 realizations of the Hindmarsh-Rose model at each of the following values of noise intensity D: 0.001 (1), 0.0025 (2), 0.005 (3), 0.025 (4), 0.0375 (5), and 0.05 (6). Other parameters are as in Fig. 3. Only the lower frequency part of the spectra is shown on these lin-log plots.

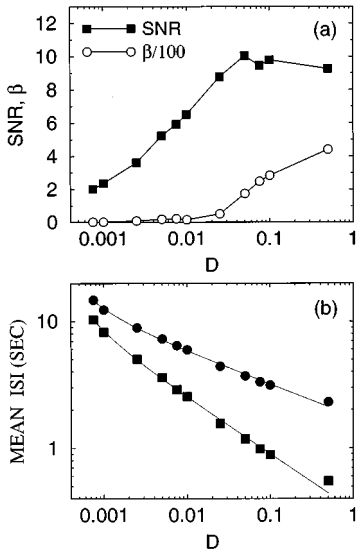

FIG. 7. (a) Signal-to-noise ratios and β vs D for the Plant model. We use $\Phi_{\mathrm{SNR}} = 10 \log_{10}(S/N)$, where $S(N)$ is the area of the f_0 peak (using 11 bins centered on f_0) above (below) the noise floor. This floor is a line joining the relative minimum about halfway through (0, f_0) to that in (f_0,2 f_0). Also, $\beta = (h f_0)/(\Delta f)$, where h and f_0 are the peak height and centroid, and Δf is the peak width at height $e^{-1/2}h$. (b) Mean interval $\langle T \rangle$ vs D using all intervals (lower curve), and neglecting the short intervals in bursts (upper curve). The data in (b) are fitted to $\langle T \rangle = C_1 D^{\nu} \exp(C_2/D)$, yielding $C_1 = 0.325$, $C_2 = 0.000208$, $\nu = -0.441$ (lower solid line), and $C_1 = 1.763$, $C_2 = 0.000205$, $\nu = -0.256$ (upper solid line). The cutoff between short and long ISI's was chosen equal to 700 msec.

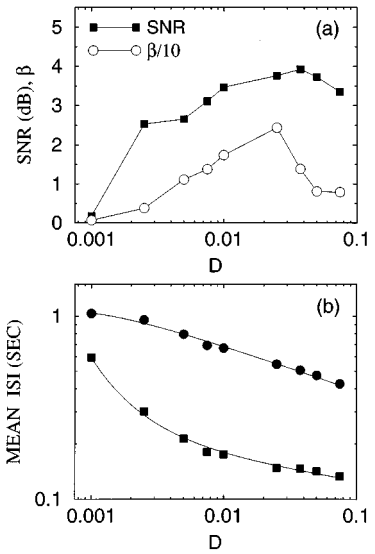

FIG. 8. (a) Signal-to-noise ratios and β vs D for the Hindmarsh-Rose model. The Φ_{SNR} and β are calculated as in Fig. 7. (b) Mean interval $\langle T \rangle$ vs D using all intervals (lower curve), and neglecting the short intervals in bursts (upper curve). The data in (b) are fitted to $\langle T \rangle = C_1 D^{\nu} \exp(C_2/D)$, yielding $C_1 = 0.0957$, $C_2 = 0.00103$, $\nu = -0.115$ (lower solid line), and $C_1 = 0.221$, $C_2 = -0.000162$, $\nu = -0.248$ (upper solid curve). The cutoff between short and long ISI's was chosen equal to 150 msec.

In our study, all spikes were used to calculate the spike train power spectra. The SNR for the slow wave case in Fig. 7(a) is seen to exhibit the familiar SR maximum as a function of D *without external forcing*, i.e., autonomous stochastic resonance. Past the maximum, the decrease in SNR appears to be slow. Simulations for $D>1.0$ are problematic and are not presented here, as spike size and shape vary enough to make the definition of threshold ambiguous. In contrast to the external forcing case [1], the SNR drop at high D in this model is also due to the disruption by noise of the coherence of the autonomous slow wave. Our computations also show that, for skipping from a slow wave, β goes through a maximum at a much larger value of D than that for the SNR (not shown in Fig. 7). Hence, β does not appear to be useful to characterize the autonomous stochastic resonance. This is likely a consequence of the robustness of the slow internal time scale in this class of bursting neurons, and of the fact that β does not directly take into account the noise floor around the signal peak.

In contrast, for the HR model, the absence of a self-oscillating slow subsystem along with the influence of the saddle-node bifurcation yields lower SNR values [Fig. 8(a)]. However, for this class of spike-driven bursters, both the SNR and β can be used to characterize the resonance, as both go through a maximum near similar values of D. Note that the small peaks flanking the fundamental peak in Fig. 6(a), present for all the noise levels studied, increase the uncertainty in our SNR estimate.

We have not studied SR by comparing time scales of the slow wave (Plant) or of the noise-induced limit cycle (HR) with the mean firing rate in the absence of these rhythms [19,23], since altering parameters to ''turn off'' these oscillations and compute a ''spontaneous'' firing rate will affect stability properties. Also, although the variation of ISIH peak heights with D is nonmonotonic, it does not exactly follow the *bona fide* resonance for simple bistable systems [19]. Noise likely samples other behaviors of these complex models, which alter the smooth progression of statistics with D.

V. CHARACTERIZATION OF THE FIRING STATISTICS

Analysis of the dependence of the mean interval $\langle T\rangle$ and of the SNR on D can provide insight into the residence-time statistics, and thus into the nature of the noise activation to threshold for these complex dynamical systems. A recent review of such questions for simple neuron models can be found in [14]. The mean interval is plotted against D for the Plant model in Fig. 7(b) and for the HR model in Fig. 8(b). In both cases, results with and without inclusion of the short intervals inside groups of spikes (''bursts'') are presented. When these short intervals are excluded, the remaining intervals represent the residence time in the nonfiring state. When the short intervals are considered, the residence-time interpretation implies that the system returns to the nonfiring state after each spike, rather than after each group of spikes. Inclusion of the short intervals lowers the $\langle T\rangle$ values, and also changes the slope and curvature of the $\langle T\rangle$ versus D relationships.

We have found that, in the range of model parameters where autonomous SR occurs, an increase in D produces a decrease in $\langle T\rangle$, as expected for subthreshold dynamics. For the slow wave case in Fig. 7(b), the data are well fitted to a relationship of the form

$$\langle T\rangle = C_1 D^{\nu}\exp(C_2/D), \tag{10}$$

shown as the solid lines. For the HR case in Fig. 8(b), the curves are also well fitted to this expression, yet the situations with and without the short intervals appear to be qualitatively different. This may be due to the uncertainties on the computed values of the mean ISI's. Note that for HR with short intervals excluded, the fit is not physically meaningful at small noise, where the mean interval goes to zero instead of infinity. This is due to the uncertainty on the small value of C_2. However, these data are also well fitted by a simple power law, with $\nu=-0.207$, $C_1=0.257$, and $C_2=0$ (not shown), which has the proper behavior at small and large noise. Further, this is compatible with the power law dependence (although with a different exponent $\nu=-1/3$) of the mean first passage time found for a simple one-dimensional model of the center manifold dynamics for a system near a saddle-node bifurcation [9].

The fact that the above expression Eq. (10) provides a proper fit to the data implies one of many possibilities. For example, one can follow a simple analysis in which the approximate time-dependent Kramers rate, normally used for external forcing [24,25], is written rather in terms of the phase θ of an autonomous oscillation,

$$\alpha(\theta) = \exp[-(U/D)(1-\eta\cos\theta)], \tag{11}$$

where U is a constant representing an effective barrier height or threshold for the spiking process (i.e., for the fast dynamics). In the HR case, the autonomous oscillation is the noise-induced limit cycle, while in the Plant case, it is the slow wave. This mean rate, which can be viewed as a mean firing rate (in spikes per second), is well approximated by the reciprocal of $\langle T\rangle$, this average being computed across many realizations (the mean rate and $\langle T\rangle$ are identical if the first spike corresponds with the beginning of the averaging period). The average of $\alpha(\theta)$ over one oscillation cycle is $\alpha_0\equiv\langle\alpha(\theta)\rangle_t=\exp(-U/D)I_0(z)$, where $z\equiv U\eta/D$ and I_0 is the modified Bessel function of order zero. In our study, it is clear that $\eta<1$, since the dynamics are subthreshold, a condition required to see stochastic resonance in the formalism of Ref. [25]. However, it is not clear whether z is small, of order one, or large. If z is large (in practice, for $z>2$), the asymptotic expansion for $I_0(z)$ yields

$$\alpha_0 \approx \frac{1}{\sqrt{2\pi}}\exp[-U(1-\eta)/D]\left(\frac{D}{U\eta}\right)^{1/2}. \tag{12}$$

Thus, the mean rate α_0 would be approximated by Eq. (10) with $\nu=-0.5$, and $C_2=U(1-\eta)>0$. For the Plant model, there is qualitative agreement with this analysis, since we find $\nu=-0.44$ when the short intervals are counted, and also a positive value for C_2.

Another possibility is that the Kramers rate approximation is not valid, or has a prefactor $f(D)$:

$$\alpha(t) = f(D)\exp[-(U/D)(1-\eta\cos\theta)]. \tag{13}$$

This leads to an expression for the mean rate

$$\alpha_0 = f(D)\exp(-U/D)I_0(z), \tag{14}$$

which, for $z<2$, can be approximated by $\alpha_0 = f(D)\exp(-U/D)$. This would be compatible with our fit if $z<2$ and $f(D)=D^{-\nu}$. This firing rate would further lead, using the formalism in [25], to the following expression for the SNR (Φ_{SNR}):

$$\Phi_{\mathrm{SNR}} = 10\log_{10}\left[\frac{2I_1^2(z)}{I_0(z)}\exp[-U/D]f(D)\right]. \tag{15}$$

However, this expression does not provide a very satisfying fit to our numerical data (not shown).

Intuitively, the modulated shot noise theory [25] would most likely apply to the slow wave case studied here, since this is the case where the autonomous rhythm is very robust to noise, as in cases with external forcing for which this theory was developed. Even for the Plant case, however, the behavior of the SNR as a function of D is not well fitted by this theory. This is not too surprising for the following reasons. First, that theory assumes that firing events are uncorrelated. Thus, it is not expected to predict the mid-to-high noise behavior, since the spikes tend to be strongly correlated due to bursting (i.e., the fast limit cycle dynamics), and also because the theory does not take a refractory period into account, i.e., the time after a spike during which no other spikes can occur.

Also, the theory in [25] was developed for a simple periodically modulated shot noise process, not for a complex nonlinear ionic model of bursting dynamics. In particular, when skipping occurs, there is a strong preference for firing near a given phase of the autonomous oscillation, mainly because of the fast limit cycle dynamics. This should be contrasted with a more continuous modulation of a firing rate, implicit in the modulated stochastic Poisson point process formulation. This is obvious from the time series in Figs. 1 and 3. Thus, in the case of bursting neurons, the rate is not accurately fitted by Eq. (11), since higher harmonics of the internal frequency have to be included (see, e.g., [27]). Because of the exponential nonlinearity, these harmonics in turn affect the value of the amplitude of the fundamental component, which will then, in the formalism of [25], affect the SNR. A further shortcoming of this approach, when only long intervals are considered, is the implication that at most one spike can occur during a cycle of the slow oscillation, even though the time scale of this oscillation is much larger than the refractory period. This is not expected for modulated shot noise, in which zero, one, or more spikes can occur during a cycle under these conditions. Clearly, further refinements of the theory in [25] or other theories are needed to account for the behavior of the mean firing rate and SNR for increasing noise.

VI. CONCLUSION

In summary, we have shown that autonomous stochastic resonance can occur in a wide variety of neurons whose bursting dynamics fall into two distinct classes. Our study also investigates stochastic resonance in a full ionic description of neural firing. The study of such models with stochastic forcing is essential to test more refined hypotheses regarding the nature of the noise (e.g., additive noise currents, and/or synaptic events, and/or conductance fluctuations) in real neurons.

It is important to realize that the motivation to study the periodicity of the spike trains in the stochastic Plant and HR models is not to find conditions under which spikes are maximally phase locked to some internal oscillation. Clearly, this can be achieved by simply considering the suprathreshold case of bursting without noise. Rather, the point here is that real receptor neurons appear to be using the subthreshold regime in order to encode certain stimuli [5,6], such as variations in temperature and/or electric fields. Our study thus focuses on the dynamics of this regime, and in particular, on how sensitive the firing pattern is to the noise, the dc bias (mainly through parameters I and i), and the bifurcation leading to the subthreshold dynamics. Fluctuations in noise inputs or dc bias, while producing relatively little change in the mean firing rate, strongly alter the phase locking of the spikes. As these quantities change in response to environmental stimuli, this sensitivity of the phase locking may be of great potential benefit for signal encoding purposes.

Finally, the behaviors as a function of D of the mean firing rate, with and without taking bursts into account, and of the ISIH's, spike train power spectra, SNR, and β uncovered in our work can serve to classify the subthreshold dynamics in real bursting neurons. Also, the addition of noise currents to the experimental preparations should produce shorter skips between firings [following Figs. 7(b) and 8(b)] if the dynamics are subthreshold to begin with. Thus, noise can serve to probe the origins of stochastically phase locked behavior in real neurons in isolation or in networks.

ACKNOWLEDGMENTS

The author wishes to thank Ivan L'Heureux, John Rinzel, Marc Courtemanche, and Gary Slater for valuable discussions. This work was supported by NSERC (Canada).

[1] K. Wiesenfeld and F. Moss, Nature **373**, 33 (1995).
[2] J. J. Hopfield, Nature **376**, 33 (1995); A. K. Engel *et al.*, Trends Neurosci. **15**, 218 (1992); R. R. Llinás, Science **242**, 1654 (1988).
[3] C. Kurrer and K. Schulten, Phys. Rev. E **51**, 6213 (1995); W. Gerstner and J. L. van Hemmen, Phys. Rev. Lett. **71**, 312 (1993); J. F. Lindner *et al.*, *ibid*. **75**, 3 (1995); P. Jung and G. Mayer-Kress, *ibid*. **74**, 2130 (1995).
[4] H. L. Bryant and J. P. Segundo, J. Physiol. (London) **260**, 279 (1976); Z. F. Mainen and T. J. Sejnowski, Science **268**, 1503 (1995).
[5] H. Braun, H. Wissing, K. Schäfer, and M. C. Hirsh, Nature **367**, 270 (1994).
[6] A. Longtin and K. Hinzer, Neural Comput. **8**, 217 (1996).
[7] H. Gang, T. Ditzinger, C. Z. Ning, and H. Haken, Phys. Rev. Lett. **71**, 807 (1993).

[8] W. J. Rappel and S. H. Strogatz, Phys. Rev. E **50**, 3249 (1994).
[9] D. Sigeti and W. Horsthemke, J. Stat. Phys. **54**, 1217 (1989).
[10] J. Rinzel and Y. S. Lee, in *Nonlinear Oscillations in Biology and Chemistry*, edited by H. G. Othmer, Lecture Notes in Biomathematics Vol. 66 (Springer-Verlag, Berlin, 1986), p. 19.
[11] R. E. Plant, J. Math. Biol. **11**, 15 (1981).
[12] J. L. Hindmarsh and R. M. Rose, Proc. R. Soc. London B **221**, 87 (1984).
[13] D. Hansel and H. Sompolinsky, Phys. Rev. Lett. **68**, 718 (1992).
[14] C. E. Smith, in *Single Neuron Computation*, edited by T. McKenna, J. Davis, and S. F. Zornetzer (Academic, San Diego, CA, 1992), p. 561.
[15] M. V. Mascagni, in *Methods in Neuronal Modeling*, edited by C. Koch and I. Segev (MIT Press, Cambridge, MA, 1989), p. 439.
[16] R. F. Fox, I. R. Gatland, R. Roy, and G. Vemuri, Phys. Rev. A **38**, 5938 (1988).
[17] J. Rinzel and Y. S. Lee, J. Math. Biol. **25**, 653 (1987).
[18] T. Zhou, F. Moss, and P. Jung, Phys. Rev. A **42**, 3161 (1990); L. Gammaitoni, F. Marchesoni, E. Menichella-Saetta, and S. Santucci, Phys. Rev. Lett. **62**, 349 (1989); *ibid*. **71**, 3625 (1993).
[19] L. Gammaitoni, F. Marchesoni, and S. Santucci, Phys. Rev. Lett. **74**, 1052 (1995).
[20] E. J. Bayly, IEEE Trans Bio-Med. Eng. **15**, 257 (1968); J. C. Coggshall, Kybernetik **13**, 30 (1973).
[21] A. S. French and A. V. Holden, Kybernetik **8**, 165 (1971).
[22] K. Wiesenfeld, J. Stat. Phys. **38**, 1071 (1985).
[23] A. Bulsara, S. Lowen, and C. Reese, Phys. Rev. E **49**, 4989 (1994).
[24] W. M. Siebert, Proc. IEEE **58**, 723 (1970).
[25] K. Wiesenfeld, D. Pierson, E. Pantazelou, C. Dames, and F. Moss, Phys. Rev. Lett. **72**, 2125 (1994).
[26] P. Jung and P. Hänggi, Phys. Rev. A **44**, 8032 (1991).
[27] D. H. Johnson, Ph.D. thesis, Massachusetts Institute of Technology, Cambridge, Massachusetts, 1974.